Langasite-based Microbalance for Determination of the Non-stoichiometry in Praseodymium-Cerium Oxide Thin Films at Elevated Temperatures

Seba... *Fritze*
Clausthal University of Technology, search and Physical Technologies,
Am Stolle... *Germany*
Sebasti... *sthal.de*

Abstract:

The oxygen partial pressure dependent non-stoichiometry of praseodymium-cerium oxide thin films ($Pr_{0.1}Ce_{0.9}O_{2-\delta}$, PCO) is investigated at temperatures between 700 and 900 °C. The non-stoichiometry of PCO is determined gravimetrically using a high-temperature microbalance consisting of piezoelectric langasite ($La_3Ga_5SiO_{14}$) resonators. Shifts of the resonance frequency are correlated with mass changes caused by oxygen incorporation/release using the Sauerbrey equation and converted into the oxygen non-stoichiometry of PCO.

Chemical and mechanical properties of the PCO films might influence the resonance frequency. Single-side deposition of PCO onto the resonators results in calculated non-stoichiometry values which exceed literature data for bulk PCO. A potential explanation is mechanical bending of the resonators due to thermo-chemical expansion. Resonators coated on both sides with PCO show smaller frequency shifts corresponding to a non-stoichiometry of up to $\delta = 0.07$, which are close to literature data.

Key words: Microbalance, high-temperature sensor, piezoelectric resonator, thin films, oxygen non-stoichiometry, oxygen ion pump

Motivation

In general, metal oxide thin films are used in electronic devices, e.g. MEMS (SiO_2, Al_2O_3), micro-batteries ($LiMnO_2$) or sensors (SnO_2, TiO_2, etc.). Metal oxides, particularly those containing transition metals or rare earth ions with multiple oxidation states, can achieve considerable oxygen non-stoichiometry which impacts the materials properties [1]. Therefore, the investigation of the non-stoichiometry in metal oxide thin films is of major interest to widen its applicability range.

Praseodymium-cerium oxide (PCO) is a promising material for oxygen storage in three-way catalysts, for cathodes of solid oxide fuel cells [2] or for mass dependent gas sensing applications [3]. Especially for the latter two applications, PCO is operated in the form of thin films at temperatures above 500 °C.

So far, numerous investigations focus on bulk samples but the results cannot be transferred to thin films or porous samples due to their higher surface to volume ratio. The enthalpy of reduction is lower for thin films. As a result, the non-stoichiometry of thin films exceeds bulk values [4]. Nevertheless, the correlation of oxygen non-stoichiometry and defect mechanisms in thin films are not fully understood yet, especially in the medium oxygen partial pressure range (approximately 10^{-6} bar to 10^{-15} bar). Consequently, further investigations are required.

Conventional thermogravimetric analysis of PCO films is not feasible due to the low sample mass. A quartz crystal microbalance enables to detect mass changes in the order of nanogram, but the phase transformation from α- to β-quartz at 573 °C prevents high-temperature measurements. In addition, material-related losses in α-quartz limit the operation for sensor application to about 450 °C [5]. Therefore, Y-cut langasite ($La_3Ga_5SiO_{14}$, LGS) single crystals are chosen as a high-temperature stable piezoelectric transducer. LGS is a quartz-isomorph which shows no phase transformation up to its melting point at 1470 °C. Most important, LGS can be piezoelectrically excited to bulk acoustic shear waves up to temperatures close to its melting point [6, 7, 8].

Defect Chemistry of PCO

The defect chemistry of $Pr_xCe_{1-x}O_{2-\delta}$ can be described by a model presented e.g. in [2]. The non-stoichiometry depends on the equilibrium

between the oxygen in the lattice and the surrounding gas atmosphere as well as the oxidation pairs Pr^{3+}/Pr^{4+} and Ce^{3+}/Ce^{4+}. The incorporation/release of oxygen follows eq. (1) given here using the Kröger-Vink notation.

$$2Pr_{Ce}^{x}+O_{O}^{x} \rightleftharpoons 2Pr_{Ce}^{'}+V_{O}^{..}+1/2\ O_{2(g)} \qquad (1)$$
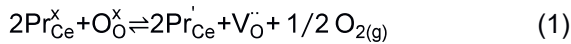
The p_{O2} dependent oxygen vacancy concentration $[V_{O}^{..}]$ and, therefore, the non-stoichiometry can be divided in three different regimes with respect to the dominating defects. At high p_{O2}, the release of oxygen is compensated by reduction of Pr^{4+} to Pr^{3+} resulting in eq. (2)

$$[V_{O}^{..}] \sim p_{O2}^{-1/6} \qquad (2)$$

At medium p_{O2}, when all Pr ions are trivalent, the oxygen vacancy concentration is fixed to fulfill the neutrality condition. At low p_{O2}, Ce^{4+} starts to reduce to Ce^{3+} and even more oxygen is released. For this work, the first and second regime are of particular interest. The non-stoichiometry δ is defined in eq. (3)

$$\delta = [V_{O}^{..}]/[Pr_{0.1}Ce_{0.1}O_{2}] \qquad (3)$$

Langasite-based Microbalance

Applying an AC voltage close to the mechanical resonance frequency of a piezoelectric Y-cut LGS single crystal excites thickness shear bulk acoustic waves [5]. Thereby, platinum/rhodium key hole shaped films deposited via pulse laser deposition serve as electrodes. LGS resonators, layer sequences and dimensions are shown Fig. 1. The deposition of mass Δm in form of a film or a change in stoichiometry of a thin film already deposited onto the resonator shift the resonance frequency (Δf) [9]. Eq. (4) is valid for mass changes up to 2 % of the resonators mass if no other effects impact the resonance frequency.

$$\Delta f/f = - \Delta m/m \rightarrow \Delta m = -A\ \Delta f/S \qquad (4)$$

In eq. (4), A is the effective resonator area and S ($S = -A\ \partial f/\partial m$) the mass sensitivity [5].

The frequency at the conductance maxima (series resonance frequency $f(G_{max})=f_{res}$) is tracked since it is independent of stray capacities [5]. In addition, the conductance spectra in the vicinity of the resonance frequency can be approximated by a Lorentzian function [8], which is beneficial for data evaluation. Since the resonance frequency is strongly temperature dependent ($\partial f_{res}/\partial T \sim$ 280 Hz K^{-1} at 600 °C for a 5 MHz resonator), temperature fluctuations of even 0.01 K could overwhelm the signal of interest. Therefore, internal temperature compensation according to [5] is applied. It uses the resonance frequency of different vibrational modes (e.g. 1st and 3rd) to calculate a temperature compensated resonance frequency f_{IC}, see eq. (5).

$$f_{IC}(m,...)=f^{[1]}(T,m,...)-\frac{c^{[1]}}{c^{[3]}}f^{[3]}(T,m,...) \qquad (5)$$

In eq. (5), $c^{[1]}$, $c^{[3]}$ are the temperature coefficients of the fundamental mode and the 3rd overtone, respectively. As a consequence, the temperature compensated mass sensitivity S_{IC} of the resonator needs to be recalculated, see eq. (6).

$$S_{IC}=S^{[1]}\left(1-3\frac{c^{[1]}}{c^{[3]}}\right) \qquad (6)$$

The mass resolution R depends on the mass sensitivity S and the accuracy of the resonance frequency determination. Taking the experimental conditions into account (thin-film diameter: 5 mm, 5 MHz resonator at 700 °C: $\Delta f^{[1]}$ = ±3 Hz [5] and Δf_{IC} = ± 9 Hz) the mass resolution is about 180 ng. Stable operation of LGS is ensured in hydrogen containing atmospheres down to oxygen partial pressure of 10^{-20} bar and 10^{-13} bar at 600 °C and 800 °C, respectively [5].
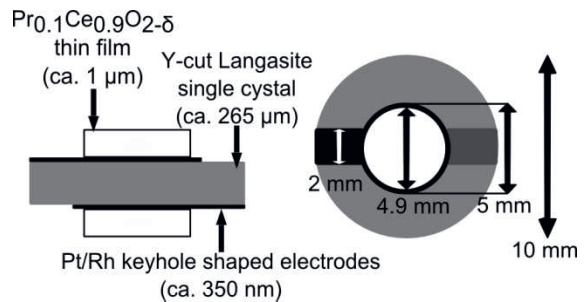

Fig. 1. Layers and dimension of a resonator; LGS single crystal, electrodes and PCO thin film.

Experimental

Polished Y-cut LGS single crystals are purchased from SICCAS (China). Platinum electrodes and PCO films are deposited by pulsed laser deposition using a KrF-Excimer laser (248 nm, COMPex, Lambda Physics, Germany). The PCO targets are prepared by stoichiometric mixtures of Pr_6O_{11} (99.9 %, Matek GmbH, Germany) and $Ce(IV)O_2$ (99.99 %, Chempur GmbH, Germany) powders which are uniaxially pressed with 55 MPa and sintered at 1350 °C. Film thicknesses are measured by profilometry using a stylus profiler XP2 (Ambios Technologies, USA).

Crystal structure of the PCO thin films is confirmed by X-Ray diffractometry (XRD) using a Siemens D5005 (Siemens AG, Germany) with a copper cathode. The set up matches the Bragg-Bretano geometry. A Nickel filter decreases the

intensity of the $Cu_{k-\beta}$ radiation. The resolution is 0.01°.

An oxygen ion pump based on yttrium stabilized zirconia enables the precise adjustment of p_{O2} in the range between 0.2 and 10^{-24} bar. Oxygen ion transport is driven by a pump current. A sensor in the vicinity of the sample enables PID control of the p_{O2} with an accuracy of $\Delta\log(p_{O2}/\text{bar}) < 0.02$ [11]. The set up of the system is shown in fig 2. The main advantage of the oxygen ion pump is the precise adjustment of the oxygen partial pressure in the medium p_{O2} range, which is interesting for sensors in regard of the application limit. Commonly, high p_{O2} are adjusted by mass flow control of oxygen and e.g. nitrogen or argon and low p_{O2} by buffer gas mixtures, e.g. H_2/H_2O, but medium p_{O2} are not easily accessible. The oxygen ion pump is connected to the gas reservoir (Argon (99.996 %), 5 % H_2/Ar (99.99 %) and oxygen (99.5 %) for $p_{O2} > 10^{-3}$ bar). Mass flow controller (MKS Instruments, Germany) guarantees a constant gas flow of 20 $cm^3 min^{-1}$.

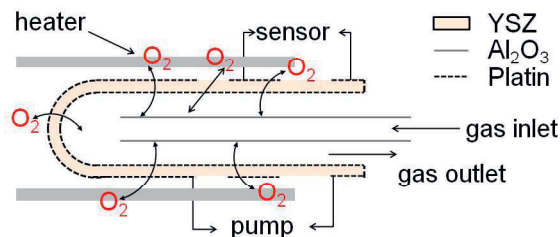*Fig. 2 Set-up of the oxygen ion pump (acc. to [11]).*

The p_{O2} dependent non-stoichiometry is measured at 700 and 900 °C in a gas tight tube furnace. A thermocouple (type B) and an oxygen sensor are installed in the vicinity of the resonator to control temperature and p_{O2}. The piezoelectric resonators are mounted in an alumina sample holder. A network analyzer (E5100 A, Agilent, USA) acquires the impedance spectra of the resonators. For the measurement of the resonance frequency, a three point calibration (open, shot and resistance of 47.3 Ω) is applied. Computer software allows an automatic tracking of the resonance frequency. All spectra contain 400 data points. The p_{O2} is varied stepwise between 10^{-1} bar and 10^{-8} bar. Each p_{O2} is held for 10-20 h to accomplish a steady state condition for the resonance frequency. The resonance frequency, oxygen partial pressure and temperature are measured every 10-15 s.

A scheme of the data recording and evaluation is given in fig. 3.

Results and Discussion

Tab. 1 summarizes the key sample properties, i.e. film mass, film thickness and temperature compensated mass sensitivities of the resonators. In this context, the term "sample" refers to the resonator with the thin film. Resonators 1 and 2 are coated on side, only. Resonator 3 is coated on both sides (see tab. 1). Temperature coefficients are obtained by a linear fit in a temperature range of ±5 K of the measurement temperature.

Tab. 1: Film mass and thickness of PCO and temperature compensated mass sensitivity of the resonators.

Sample	Film mass [µg]	Total film thickness [nm]	S_{IC} [cm^2 Hz µg^{-1}]
1	63.5	642 ± 45	-18.1 (700 °C)
2	67.8	563 ± 47	0.7 (900 °C)
3	117.1	1995 ± 110	-27.1 (700 °C) 4.3 (900 °C)

Calculated densities ($\rho = \Delta m/A_R \cdot d$) with A_R is the thin film radius applying Sauerbrey model and d is the film thickness) of the thin film are 6.9 g cm^{-3} in average and therefore close to the bulk value (7.31 g cm^{-3} [2]). Profilometry results in a surface roughness of about 100 nm which indicates high surface areas.

XRD shows a diffraction peak at about 28.6°, which can be assigned to the (111) reflex of fluorite crystal structure of PCO [12]. The peak occurs after annealing the samples at 700 °C, only.

It must be noted that the temperature compensated resonance frequency f_{IC} and mass sensitivity S_{IC} (see tab. 1) can show negative values, depending on the ratio of the temperature coefficients of the corresponding vibrational modes. Nevertheless, the mass change is reflected correctly. Fig. 4 shows the resonance frequency (1st and 3rd vibrational mode) of a both-sided coated resonator as function of temperature in air. The resonance frequencies follow a parabolic dependence (red lines). Differences between the heating and cooling are insignificant.
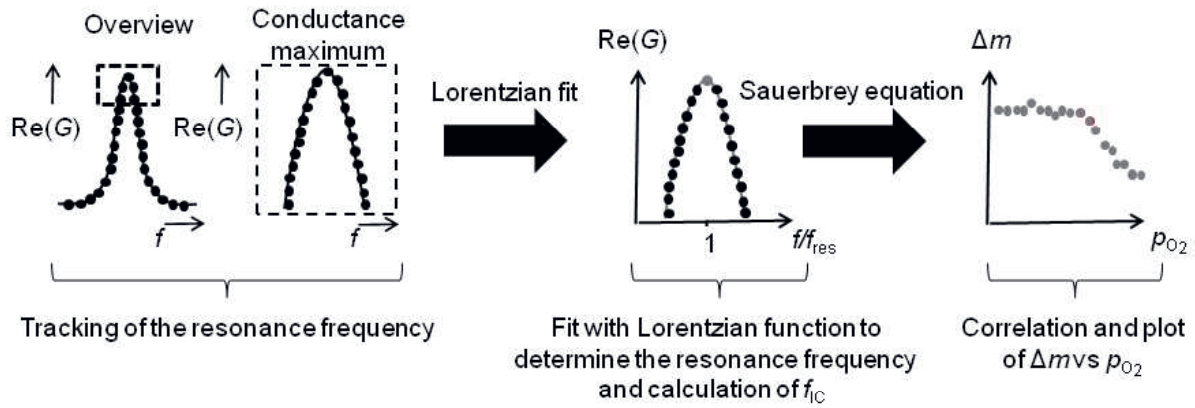
Fig. 3 Scheme of the data recording and evaluation

Therefore it can be concluded that temperature effects on the PCO thin film are reversible in air.
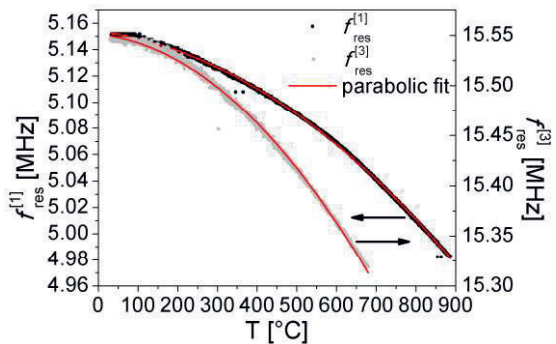

Fig. 4 Temperature dependence of the 1st and 3rd vibrational mode of a both-sided coated resonator

Changes of the oxygen partial pressure result in a sudden change of the resonance frequency, but it takes 10-20 h until steady-state conditions are achieved. Furthermore, the fluctuation of the data causes an uncertainty in determination of the evaluation of steady-state conditions.

Samples 1 and 2 show higher fluctuations of the resonance frequency, especially for the calculated internal compensated resonance frequency. The internal compensated mass sensitivities (see tab.1) are low (e.g. the mass sensitivity of a 5 MHz resonator is about 32.1 cm^2 Hz µg^{-1} [5]) due to the ratio of $c^{[1]}$ and $c^{[3]}$. As a result, applying eq. (6) results in higher errors. Calculated mass (and non-stoichiometry) changes exceed literature data. For sample 2, the calculated mass loss during decreasing the p_{O2} to 10^{-8} bar exceeds the film mass itself. Therefore, applying Sauerbrey equation is obviously a wrong interpretation and a more comprehensive examination for influences on the resonance frequency is required. A potential explanation might be the thermo-

chemical expansion of PCO, which results in mechanical stress at the interface of the electrode and the PCO thin film [1]. A Bending of the planar resonator could, potentially, cause a resonance frequency shift much larger than for pure mass changes.

Resonators coated on both sides show results which are at 700 °C in good agreement with literature data. In contrast to single-side coated resonators, bending of the resonators and, therefore, additional frequency shift is minimized.

The measurement at 900 °C results again in too high values for the mass losses due to the low internal compensated mass sensitivity. Evaluation of the 1st mode and f_{IC} results in mass changes up to 10 µg and 90 µg, respectively. This indicates that the impact of thin films stress/bending of the resonator is different for the 1st and 3rd mode.

Fig. 5 shows the oxygen partial pressure dependent frequency shifts and corresponding mass changes for sample 2 at 700 °C. The resonance frequency at p_{O2} = 10^{-1} bar and 700 °C is taken as the reference for further calculation. The non-stoichiometry and mass loss (according to eqs. (3) and (4)) increases initially and reaches a plateau at about 10^{-5} bar as predicted by the defect model [2]. The literature data presented in fig. 5 refer to a pure oxygen atmosphere at room temperature. The calculation of our data is done using literature data at high p_{O2} as reference.
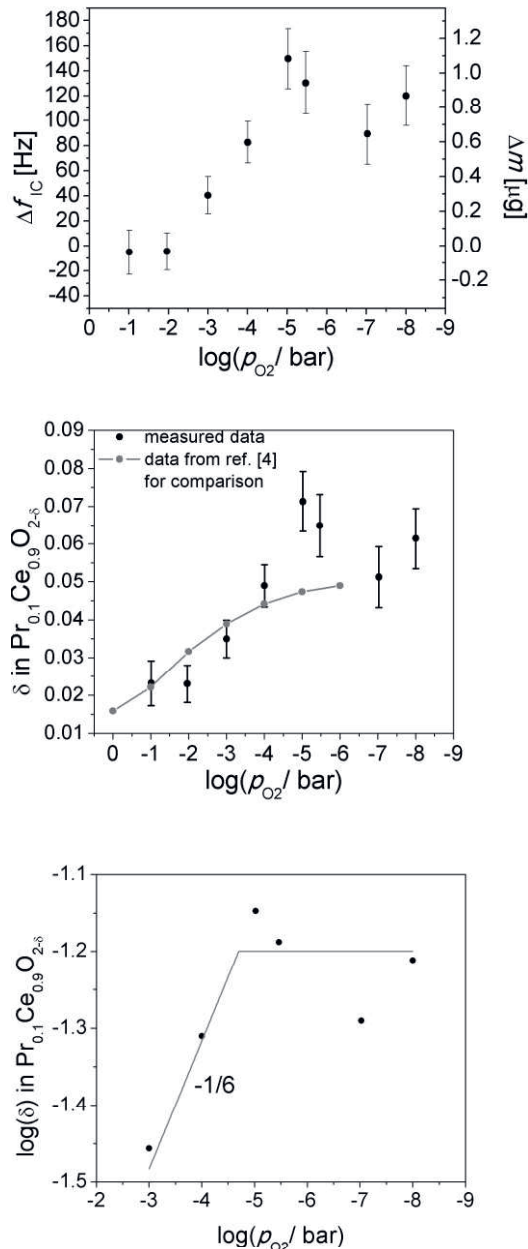
Fig.5. Shift of the temperature compensated resonance frequency and calculated mass changes (top) and non-stoichiometry (middle) of resonator 3 at 700 °C. Error bars for the oxygen partial pressure are smaller than data points. The logarithm of the non-stoichiometry in dependence of the oxygen partial pressure is given for comparison with the defect model (bottom). Data points at 10^{-1} bar and 10^{-2} bar are excluded because of errors bars include $\delta = 0$. The grey line reflects the defect model and does not represent a fit of the data.

Compared to the fundamental mode and 3rd overtone, the temperature compensated resonance frequency shows more fluctuations.

Reasons for the deviation of calculated non-stoichiometries and literature values are in ac-

cordance with the ability of thin films to show higher non-stoichiometries compared to bulk samples. The behavior results from a decreased enthalpy of reduction of praseodymium [4] and decreased activation energy for the incorporation/release of oxygen [13] in such films. Another indication is the mass loss in porous gadolinium doped ceria (bulk samples), which exceeds values for dense samples [14]. Recently, a coupling of strain, stress and non-stoichiometry in thin film PCO is presented in [1]. Non-stoichiometry results in a shift of the defect formation energies, which appears to decrease with tensile stress (up to about 750 °C) and increase with compressive stress (above 750 °C) [1]. The thermo-chemical expansion coefficient decreases with increasing temperature and the elastic modulus is greater than in bulk samples. In addition, stress relaxation and slow kinetics are observed [1]. Comprehensive stress could be a reason why measurements at 900 °C exceed reasonable values even for both side coated resonators. In addition, irreversible stresses are observed in this work and in [1] causing difficulties in data evaluation.

Summary and Conclusion

The non-stoichiometry in praseodymium-cerium oxide thin films ($Pr_{0.1}Ce_{0.9}O_{2-\delta}$, PCO) is investigated by a high-temperature stable microbalance (Y-cut langasite, $La_3Ga_5SiO_{14}$).

Mass changes of the thin film as function of the oxygen partial pressure are measured by monitoring the resonance frequency and applying Sauerbrey equation. Since the resonance frequency is strongly temperature dependent, a temperature compensation based on measuring the fundamental mode and third overtone according to [5] is applied. It is assumed that mass changes are result of release/ incorporation of oxygen.

PCO thin films are prepared by stoichiometric mixing of Pr_6O_{11} and $Ce(IV)O_2$ powders, which are uniaxially pressed and sintered at 1350 °C. The received pellets are used for pulsed laser deposition process. After a heat treatment at 700 °C in air, XRD indicates fluorite crystal structure of the thin films. The resonance frequency shows insignificant changes during heat treatment in air, indicating that thermal effects are reversible.

Calculated non-stoichiometries for thin films exceed literature values for bulk samples, which is a common phenomenon and a result of a decreased enthalpy of reduction of praseodymium and activation energy for the incorporation/release of oxygen.

Mechanical stress caused by the thin films might effect the resonance frequency. Resonators coated with PCO on both sides and measured at 700 °C show good agreement with the above mentioned literature data.

Acknowledgement

References

[1] J. Sheth, D. Chen, J. J. Kim, W. J. Bowman, P. A. Crozier, H. L. Tuller, S. T. Misture, S. Zdzieszynski, B. W. Sheldon, S. R. Bishop, Coupling of strain, stress, and oxygen non-stoichiometry in thin film $Pr_{0.1}Ce_{0.9}O_{2-\delta}$, *Nanoscale* 8, 16499-16510 (2016); doi: 10.1039/c6nr04083g

[2] S.R. Bishop, T.S. Stefanik, H. L. Tuller, Electrical conductivity and defect equilibria of $Pr_{0.1}Ce_{0.9}O_{2-\delta}$, *Physical Chemistry and Chemical Physics* 13, 10165-10173 (2011); doi: 10.1039/C0CP02920C

[3] H. Seh, H. L. Tuller, H. Fritze, Thin film Praseodymium-Cerium Oxide Langasite based microbalance gas sensor, *Journal of Electroceramics* 13, 755-778 (2004); doi: 10.1007/s10832-004-5191-y

[4] D. Chen, S. R. Bishop, H. L. Tuller, Nonstoichiometry in oxide thin films operating under anodic conditions: A chemical capacitance study of the Praseodym-Cerium oxide system, *Chemistry of Materials* 26, 6622-6627 (2014); doi: 10.1021/cm503440v

[5] H. Fritze, High-temperature bulk acoustic wave sensors, *Measurement Science and Technology* 22, 01200-012030 (2011); doi: 10.1088/0957-0233/22/1/012002

[6] D. Richter, H. Fritze, T. Schneider, P. Hauptmann, N. Bauersfeld, K.-D. Kramer, K. Wiesner, M. Fleischer, G. Karle, A. Schubert, Integrated high temperature gas sensor system based on bulk acoustic wave resonators, *Sensors and Actuators B* 118, 466-471 (2006) doi: 10.1016/j.snb.2006.04.041

[7] M. Schultz, H. Fritze, Electromechanical properties of langasite resonators at elevated temperatures, *Renewable Energy* 33, 336-341 (2008); doi: 10.1016/jrenene.2007.05.016

[8] H. Fritze, H. L. Tuller, G. Borchardt, T Fukuda, High-Temperature Properties of Langasite, *MRS Proceedings* 604, 65-70 (1999); doi: 10.1557/PROC-604-65

[9] G. Sauerbrey, Verwendung von Schwingquarzen zur Wägung dünner Schichten und Mikrowägung, *Zeitschrift für Physik* 155, 206-222 (1959)

[10] A. Bund, G. Schwitzgebel, Signal-oscillations of a piezoelectric quartz crystal in liquids caused by compressional waves, *Analytica Chimica Acta* 364, 189-194 (1998); doi: 10.1016/S0003-2670(98)00201-3

[11] M. Schulz, J. Brillo, C. Stenzel and H. Fritze, Oxygen partial pressure control for microgravity experiments, *Solid State Ionics* 225, 332-336 (2012); doi: 10.1016/j.ssi.2012.04.008

[12] K. Ahn, D. S. Yoo, D. H. Prasad, W.-W. Lee, Y.-C- Chung, J.H. Lee, Role of multivalent Pr in the formation and migration of oxygen vacancy in Pr-doped Ceria: Experimental and First-principles investigations, *Chemistry of Materials* 24, 4261-4267 (2012); doi: 10.1021/cm3022424

[13] J.J. Kim, S. R. Bishop, N. J. Thompson, D. Chen, H. L. Tuller, Investigation of nonstoichiometry in oxide thin films by simultaneous in situ optical absorption and chemical cpacitance measurements: pr-doped Ceria, a case study, *Chemistry of Materials* 26, 1374-1379 (2014); doi: 10.1021/cm403066p

[14] S. R. Bishop, K. L. Duncan, E. D. Wachsman, Surface and bulk oxygen non-stoichiometry and bulk chemical expansion in gadolinium-doped cerium oxide, *Acta Materialia* 57, 3596-3605 (2009); doi: 10.1016/jactamat.2009.04.017

[15] B. W. Sheldon, V. B. Shenoy, Space charge induced surface stress: Implication in Ceria and other ionic solids, *Physical Review Letters* 106, 216104-216108 (2011); doi: 10.1103/PhysRevLett.106.216104